Journal of the Mechanical Behavior of Biomedical Materials 89 (2019) 54–64

Contents lists available at ScienceDirect

Journal of the Mechanical Behavior of Biomedical Materials

journal homepage: www.elsevier.com/locate/jmbbm

Multi-material Ti6Al4V & PEEK cellular structures produced by Selective Laser Melting and Hot Pressing: A tribocorrosion study targeting orthopedic applications

F. Bartolomeu[a,*], M. Buciumeanu[b], M.M. Costa[a], N. Alves[c], M. Gasik[d], F.S. Silva[a], G. Miranda[a]

[a] Center for Micro-Electro Mechanical Systems (CMEMS-UMinho), University of Minho, Campus de Azurém, 4800-058 Guimarães, Portugal
[b] Cross–Border Faculty of Humanities, Economics and Engineering, "Dunărea de Jos" University of Galați, Domnească 47, 800008 Galati, Romania
[c] Centre for Rapid and Sustainable Product Development Polytechnic Institute of Leiria, Rua General Norton de Matos, Apartado 4133, 2411-901 Leiria, Portugal
[d] Department of Materials Science and Engineering, School of Chemical Technology, Aalto University Foundation, 00076 Aalto, Espoo, Finland

ARTICLE INFO

Keywords:
Ti6Al4V-PEEK
Selective Laser Melting
Hot Pressing
Multi-material
Cellular structures
Tribocorrosion

ABSTRACT

Ti6Al4V-alloy is commonly used in dental and orthopedic applications where tribochemical reactions occur at material/bone interface. These reactions are one of the main concerns regarding Ti6Al4V implants due to the generation of wear particles, linked to the release of metallic ions in toxic concentration which occurs when TiO_2 passive film is destroyed by means of wear and corrosion simultaneously. In the present study, a multi-material Ti6Al4V-PEEK cellular structure is proposed. Selective Laser Melting technique was used to produce Ti6Al4V dense and cellular structured specimens, whilst Hot-Pressing technique was employed to obtain multi-material Ti6Al4V-PEEK structures. This study investigates the tribocorrosion behavior of these materials under reciprocating sliding, comparing them with commercial forged Ti6Al4V. Open-circuit-potential was measured before, during and after sliding while dynamic coefficient of friction was assessed during sliding. The results showed an improved wear resistance and a lower tendency to corrosion for the multi-material Ti6Al4V-PEEK specimens when compared to dense and cellular structures mono-material specimens. This multi-material solution gathering Ti6Al4V and PEEK, besides being able to withstand the loads occurring after implantation on dental and orthopedic applications, is a promising alternative to fully dense metals once it enhances the tribocorrosion performance.

1. Introduction

Selective Laser Melting (SLM) is a powder bed additive manufacturing (AM) technique that allows the construction of 3D components (Xu et al., 2015; Miranda et al., 2016). In SLM a CAD model previously prepared is imported to SLM software and then sliced in several layers. According to the CAD data, a cyclic process occurs in which a powder deposition is followed by a laser scan that promotes the melting of the deposited powder (Bartolomeu et al., 2017a). The process ends when the last layer of the component is printed. Being a layer-wise fabrication technique, SLM versatility allows the production of customized products with complex geometries (Wang et al., 2016; Bartolomeu et al., 2017b). SLM has the potential to trigger material/engineering changes that can enable a new ideology in which implants are designed for each patient.

Ti6Al4V is the most widely used titanium alloy and it is also one of the most used materials on AM techniques such as SLM (Lu et al., 2016). This material is often referred as the workhorse material in the industry once it finds application in various branches of the industry (Bartolomeu et al., 2016). Ti6Al4V characteristics make this material suitable for a diversified range of high-added-value products as transports and automotive (Shunmugavel et al., 2015), electronics, aerospace and aeronautics (Kasperovich et al., 2016; Raju et al., 2015; Liu et al., 2016a) and medicine (Van Hooreweder et al., 2017; Weißmann et al., 2016). Ti6Al4V main properties can be resumed as follows: high strength, low weight, relatively low young's modulus, biological compatibility with human tissues and superior corrosion resistance (Dantas et al., 2017; Sampaio et al., 2016a). This material has the ability to form a very stable passive layer, mainly formed of TiO_2, that covers the titanium surface and provides superior biocompatibility (Buciumeanu et al., 2018). When this film layer is damaged, the repassivation process occurs very quickly (Geetha et al., 2009) when compared to stainless steel and other biomedical alloys (Geetha et al., 2009). However, Ti6Al4V has a poor wear resistance which may be responsible for

* Corresponding author.
E-mail address: flaviojorgebartolomeu@gmail.com (F. Bartolomeu).

https://doi.org/10.1016/j.jmbbm.2018.09.009
Received 13 June 2018; Received in revised form 5 September 2018; Accepted 6 September 2018
Available online 10 September 2018
1751-6161/

accelerate the corrosion damage (Licausi et al., 2013; Runa et al., 2013).

The tribocorrosion performance of an implant material plays a crucial role on its success (Holzwarth and Cotogno, 2012). Implant experiences tribocorrosion, which is a deterioration process that takes place at the interface of contacting surfaces, surrounded by a corrosive medium, due to the existence of relative movements (Runa et al., 2013; Souza et al., 2015a). Several studies reported evidences of surface damage caused by corrosion and wear on metallic implants, such as Ti6Al4V, in physiological mediums (Runa et al., 2013; Donell et al., 2010). The tribocorrosion process degrades materials through the combined effect of corrosion mediums and wear (Sampaio et al., 2016a). In spite of the great progress that has been achieved in biomaterials field used for implants, corrosion and wear phenomena are still reported as a failure mode of major importance (Geetha et al., 2009; Rodrigues et al., 2013; Ganesh et al., 2012; Goodman, 2007). For instance, on Ti6Al4V hip implants the wear particles generated by the sliding movements that occur in the articular joints and on the stem, have been related to tissue inflammatory reactions (Souza et al., 2015a). Geetha et al. Geetha et al. (2009)) stated that wear/corrosion are one of the most important problems that lead to implant failures.

Aiming to improve the tribocorrosion performance of the available solutions on the market, several studies have been performed on Ti6Al4V alloy, the majority of them essentially focusing the influence of different surfaces treatments, composite materials, functionally graded materials and coatings on the tribocorrosion performance (Fazel et al., 2015; Obadele et al., 2015; Buciumeanu et al., 2017a; Sampaio et al., 2016b).

Biocompatible polymers have been explored to overcome these issues related to tribological and tribocorrosion process occurring on metallic implants (Sampaio et al., 2016a; Buciumeanu et al., 2018). Poly-ether-ether-ketone (PEEK) is an attractive material to be used in biomedical applications, owing to its high chemical stability and wear and corrosion resistance when compared to Ti6Al4V alloy (Moon et al., 2009; Friedrich et al., 2011). PEEK Young's modulus (YM) of around 3.6 GPa (Moon et al., 2009; Friedrich et al., 2011), much lower than that of cortical bone (around 20 GPa (Wang et al., 2016)) hampers its use as implant material alone, allowing however, its use in multi-material metallic structures.

This work proposes a Ti6Al4V-PEEK multi-material cellular structure produced by an advanced AM technique and a highly efficient powder metallurgy route, in order to design an improved solution for dental implants and orthopedic application such as hip implants, tibial plates and spinal cages that combines the suitable mechanical properties with an improved tribological and corrosion performance.

2. Experimental procedure

2.1. Starting materials

The powder used to fabricate Ti6Al4V specimens by SLM was purchased from *SLM Solutions* (Germany). Ti6Al4V powder chemical composition and particle morphology can be seen in Table 1 and Fig. 1(a), respectively. The PEEK powder that was used to produce a Ti6Al4V-PEEK multi-material structure was purchased from *Evonik Industries* (Germany) and its particles morphology can be seen in Fig. 1(b). In this study, commercial Ti6Al4V forged alloy purchased from *Titanium Products Ltd.* (United Kingdom) was also used as group control representing the current material used on implants.

Table 1
Chemical composition of Ti6Al4V powder used to produced Ti6Al4V specimens by SLM.

Element	Ti	Al	V	C	Fe	O	N	H
wt%	Balance	6.4	3.8	0.01	0.23	0.12	0.02	0.0074

2.2. Design and production details

Fig. 2 depicts the processing overview of this study representing the production stages from the conception to the final specimens for the different types of materials investigated. In this study four different types of Ti6Al4V-based specimens were produced. Table 2 resumes the processing details and material specification. All the specimens tested have a cylindrical shape 9 mm diameter and 2.5 mm of thickness. SP1 Ti6Al4V forged specimens were cut from a Ti6Al4V bar. SP2, SP3 and SP4 Ti6Al4V specimens were produced by using a Selective Laser Melting commercial machine from *SLM Solutions* (Germany) model 125HL. The SLM processing details used to produce Ti6Al4V dense and cellular structures are presented in Fig. 3. This processing parameters (power, scan speed and scan spacing) selection was based on a previous study (Bartolomeu et al., 2016) where the most effective processing parameters were defined.

After producing Ti6Al4V cellular structures by SLM, SP4 Ti6Al4V-PEEK multi-material specimens were obtained by introducing PEEK into the holes of the structures. PEEK impregnation was carried out by using a pressure assisted technique, Hot Pressing (HP), in which pressure and temperature are simultaneously applied. Fig. 4 aims to resume the PEEK impregnation procedure. This procedure starts with Ti6Al4V cellular specimens being placed in a mold and afterwards introducing PEEK powder on the space between the Ti6Al4V specimens and the mold walls. After this, the top punch is inserted in the mold and the system is positioned inside a chamber with a vacuum atmosphere of 10^2 mbar. An initial residual pressure was applied to accommodate the PEEK powder. Then, the induction heating was started till reaching 380 °C (above the melting point of PEEK (345 °C)) using a heating rate of 80 °C/min. The temperature was decreased until 300 °C and a pressure of 25 MPa was applied and maintained for 5 s, forcing PEEK to fill the open cells of the structure. Finally, the Ti6Al4V-PEEK structures were removed from the system (Fig. 4).

2.3. Tribocorrosion tests

The tribocorrosion evaluation was performed by using a tribometer from *Bruker-UMT-2* (USA). A reciprocating ball-on-plate configuration was used in which the Ti6Al4V-based materials were the plates, while as counter parts alumina balls with 10 mm of diameter purchased from *Goodfellow* (United Kingdom) were used. Fig. 5 shows a schematic representation of the tribocorrosion test. Before starting the tribocorrosion tests, all the specimens were polished using SiC abrasive papers down to 4000 mesh and then cleaned in a ultrasonic bath in isopropyl alcohol for 15 min. Ti6Al4V specimens were fixed in an acrylic device that was attached to the tribometer. Reciprocating sliding tests were carried out with normal load of 6 N at a frequency of 1 Hz and 3 mm of stroke length in Phosphate Buffer Solution at 37 °C. These testing parameters were used in order to mimicking to some extent the temperature and the electrochemical medium found in human body.

A standard two-electrode electrochemical cell was used for the electrochemical measurements. Saturated calomel electrode (adapted from ASTM G3 – 14) was used as the reference electrode and Ti6Al4V-based specimens (SP1, SP2, SP3 and SP4) as the working electrode (Doni et al., 2013). Open circuit potential (OCP) was measured before (at least 60 min in order to assure stabilization), during (30 min) and after reciprocating sliding tests (30 min) by using a Gamry Potentiostat/Galvanostat (model Reference-600). The specific wear rate was estimated by evaluating the width of the wear tracks and mathematical equations were used assuming that the wear tracks are formed by perfect alumina ball geometry (Sampaio et al., 2016a; Bartolomeu et al., 2017c).

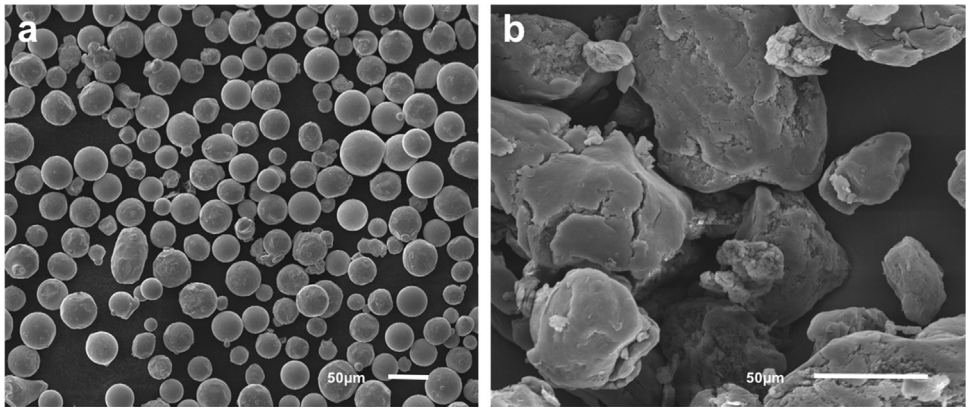

Fig. 1. SEM images of (a) Ti6Al4V and (b) PEEK powders.

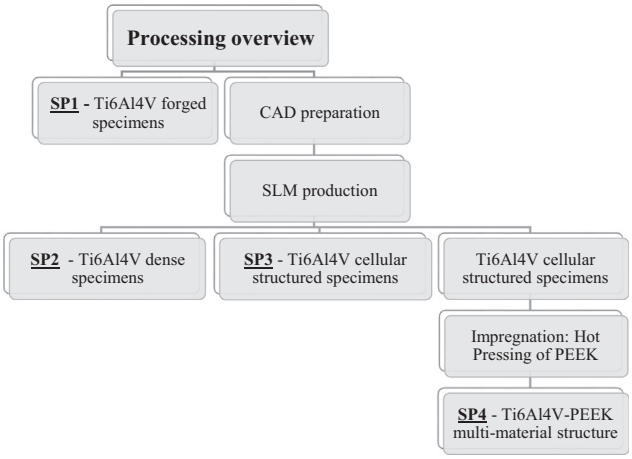

Fig. 2. Full processing representation for the specimens produced (SP1, SP2, SP3 and SP4).

Table 2
Ti6Al4V-based specimens processing and materials details.

Specimen	Processing technology	Materials specification
SP1	Forged	Ti6Al4V Dense
SP2	Selective Laser Melting	Ti6Al4V Dense
SP3	Selective Laser Melting	Ti6Al4V cellular structured
SP4	Selective Laser Melting & Hot Pressing	Ti6Al4V cellular structure-PEEK

2.4. SEM analysis and X-ray diffraction

SEM analysis was used to characterize the morphology of the powders and the Ti6Al4V-based specimens. SEM micrographs of Ti6Al4V structures (after SLM) and of Ti6Al4V-PEEK structures (after SLM/HP process) were obtained in different time points: as-built by SLM, after polishing, after polishing/acid-etching with Kroll's reagent (5% HNO_3, 10% HF and 85% of distilled water) and finally after the tribocorrosion tests. Additionally, before the tribocorrosion tests, each specimen was characterized by X-ray diffraction using Bruker AXS D8 Discover (USA) equipment. Diffraction data were collected from 10° to 80° 2θ, with a step size of 0.02° and counting time of 1 s/step.

2.5. Statistical analysis

In order to assure the repeatability of the study, tribocorrosion tests were repeated at least three times, using different specimens. The obtained experimental values (OCP, coefficient of friction and specific wear rate) are reported as the average values ± standard deviation and considering at least four tests for each condition. The tribocorrosion results were analyzed by one-way ANOVA followed by Tukey's test for multiple comparisons with a significance level of $p < 0.05$.

3. Results and discussion

3.1. Characterization prior to testing

In this study, SLM technique was exploited in order to produce Ti6Al4V specimens based on CAD data. Fig. 6(a) and (c) shows the CAD models while in Fig. 6(b) and (d) shows SEM images of the as-build Ti6Al4V dense and cellular structured specimens. Fig. 7 shows a SEM image of the multi-material Ti6Al4V-PEEK cellular structure produced in this study.

When comparing the CAD drawing with the produced Ti6Al4V cellular structures some dimensional differences can be detected. On the CAD file, the size of the open-cells is 400 µm and the distance between the open-cells (walls thickness) is 300 µm. On the produced specimens the average size of the open-cells were reduced 100 µm as result of an increase of 100 µm on the wall thickness. F. Bartolomeu et al. Bartolomeu et al. (2017a) explained these deviations in their study where Ti6Al4V cellular structures with different open-cells sizes (from 100 to 400 µm) were produced by using the same equipment with the same processing conditions.

On Fig. 8, SEM images of the top surfaces of polished SP1, SP2, SP3 and SP4 specimens before the tribocorrosion tests can be seen. Fig. 8(a) and (b) show the forged (SP1) and SLM (SP2) dense Ti6Al4V specimens, respectively. Fig. 8(d) shows the top surface of the multi-material Ti6Al4V-PEEK cellular structure. Additionally, Fig. 8(e) depicts a cross-section of the multi-material Ti6Al4V-PEEK cellular structure, where a well-succeeded impregnation and effective mechanical interlocking

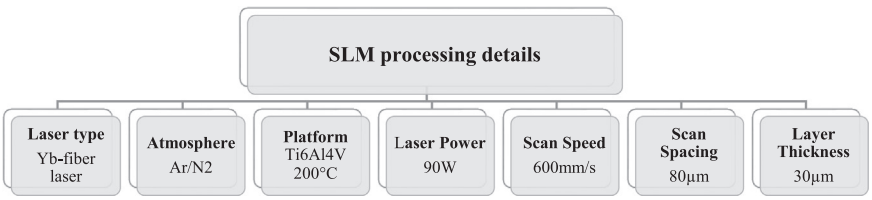

Fig. 3. Selective Laser Melting processing details used to produce Ti6Al4V specimens (SP2, SP3 and SP4).

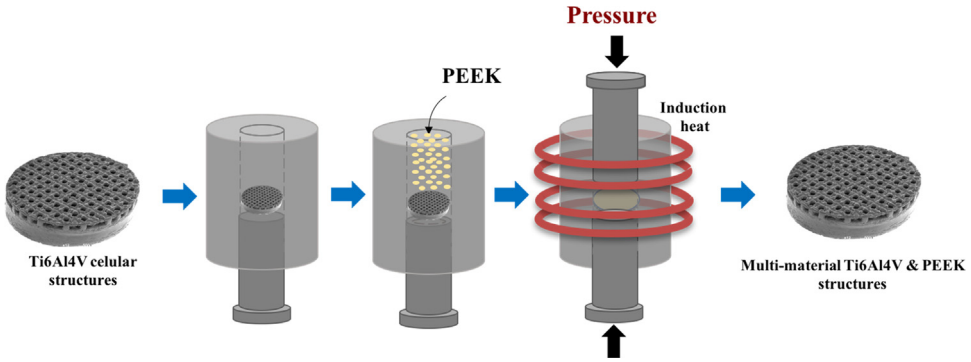

Fig. 4. Hot Pressing procedure to impregnated PEEK into the Ti6Al4V cellular structures.

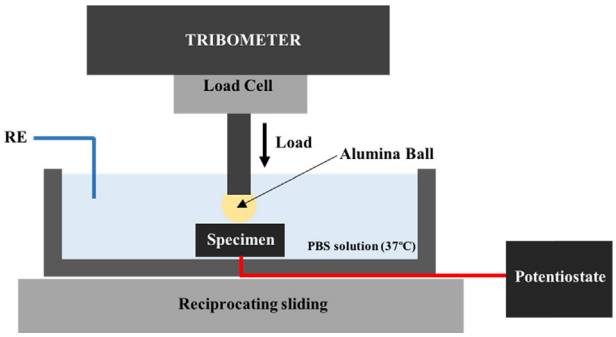

Fig. 5. Schematic representation of the tribocorrosion test.

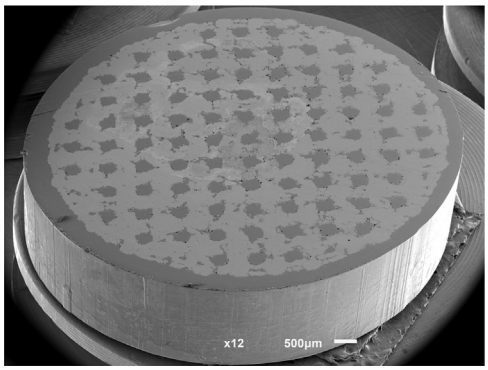

Fig. 7. SEM image of as polished Ti6Al4V-PEEK multi-material cellular structure (SP4).

between PEEK and the Ti6Al4V structure is demonstrated, validating the experimental procedure proposed.

In this study, Ti6Al4V-based specimens produced by forging, Selective Laser Melting and Selective Laser Melting /Hot Pressing were studied. The use of different processing routes influences the microstructural features of Ti6Al4V alloy (Murr et al., 2009; Song et al., 2015). Ti6Al4V is an α–β alloy (Raju et al., 2015) that contains 6 wt% of Aluminum (acting as α-phase stabilizer) and 4 wt% of Vanadium (acting as β-phase stabilizer) (Kasperovich et al., 2016; Donachie, 2000). The β-transus temperature is around 995 °C (equilibrium conditions) and above this temperature this alloy becomes 100% β–phase (Murr et al., 2009).

Fig. 9 shows SEM micrographs of the top surfaces of the polished and acid-etched Ti6Al4V-based specimens studied. In fact, before analyzing Fig. 9 it is important to clear that Ti6Al4V microstructure is decidedly associated with the cooling rate induced by the processing

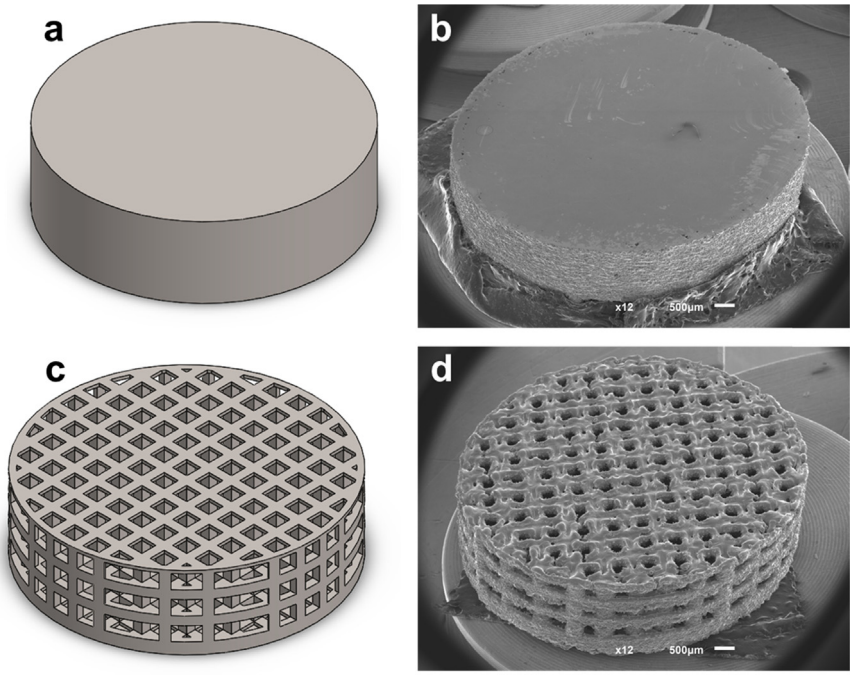

Fig. 6. Ti6Al4V dense and cellular structured specimens: CAD images ((a) and (c)) and as-built SEM images ((b) and (d)).

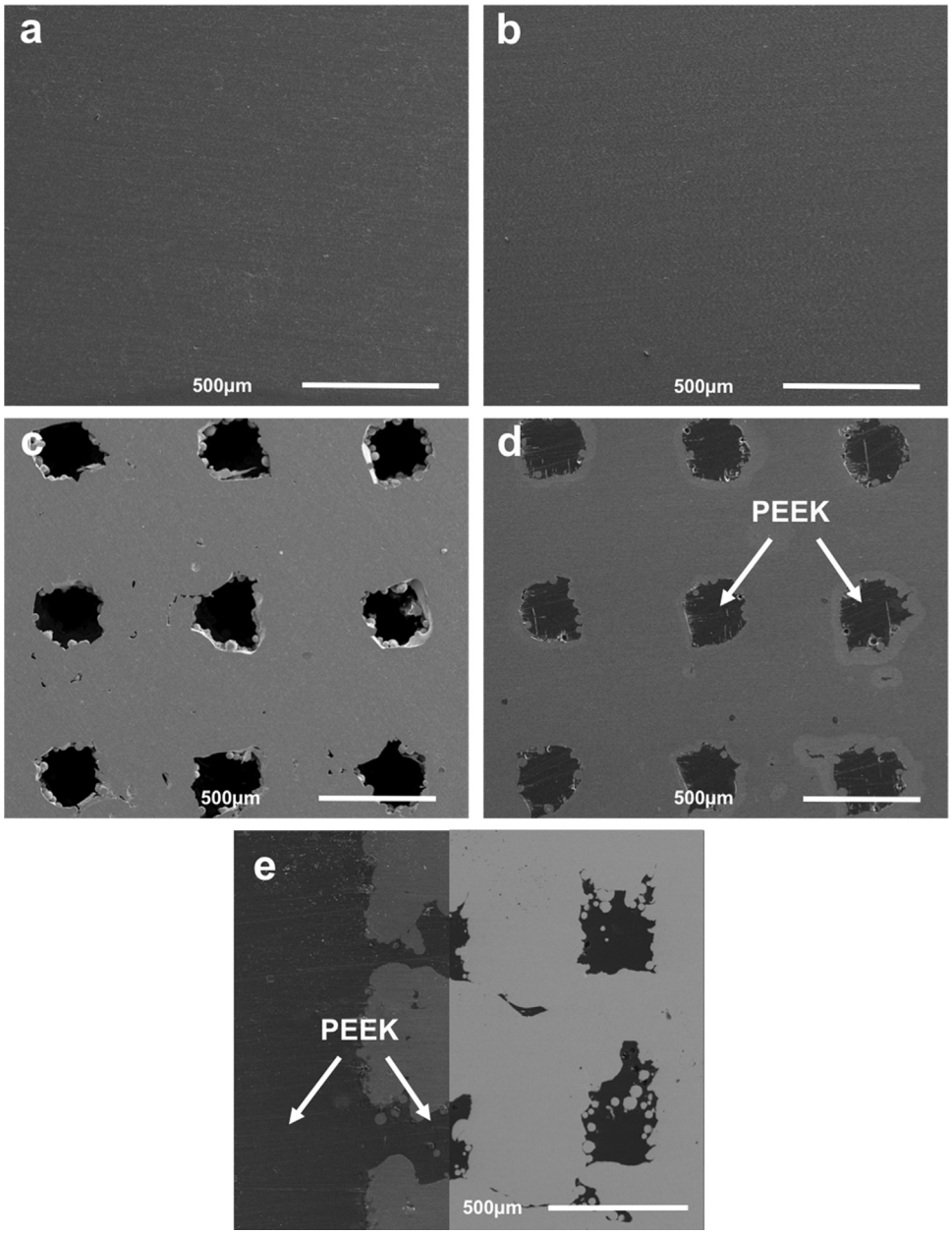

Fig. 8. (a) SP1, (b) SP2, (c) SP3 and (d) SP4: SEM images of the top surfaces of Ti6Al4V-based polished specimens and (e) SEM image of SP4 cross section.

route from above β transus temperature (Shunmugavel et al., 2015; Raju et al., 2015). Commonly, Ti6Al4V forged components displays a α–β coarse structure once during the processing the material experiences a slow to intermediate cooling rate (Jovanović et al., 2006; Toh et al., 2016). The SEM images of SP1 specimen (forged Ti6Al4V) from Fig. 9(a) supports the above-mentioned event, by displaying a typical coarse microstructure. On other hand, when the cooling rate is sufficiently fast, β-phase undergoes a diffusionless transformation to martensitic α′-phase (Bartolomeu et al., 2016). Fig. 8(b), (c) and (d) display SEM images of SLM SP2, SP3 and SP4, where a fine acicular morphology can be seen, corresponding to the α' martensitic phase (Liu et al., 2016b). This was expectable once the cooling rates experienced by this material during SLM is extremely fast (10^3–10^6 K/s) (Thijs et al., 2010).

SEM images of the acid-etched SP2, SP3 and SP4 present in Fig. 9(b), (c) and (d), show a needle-like morphology (Bruschi et al., 2017). SP4 images (Fig. 9(d)) allows concluding that the Hot Pressing procedure used to impregnate the PEEK into the holes of the Ti6Al4V cellular structure do not lead to substantial visible microstructural differences on the Ti6Al4V.

Figs. 10 and 11 show the X-ray diffraction spectra of the starting materials (Ti6Al4V and PEEK powder) and also of SP1, SP2, SP3 and SP4 specimens, respectively. as polished. Both Hexagonal Close-packed structure (α-phase) and Body-Centered Cubic structure (β-phase) were detected on Ti6Al4V starting powder and also on all the Ti6Al4V-based specimens. It is important to highlight that α and α′ (martensite) phases have the same crystalline structure and very similar lattice parameters. Then, the HCP peaks detected on SP2, SP3 and SP4 can be attributed both to α and α′ phases (Bartolomeu et al., 2017c; Zhang et al., 2014). However, the microstructural assessment made using SEM images (Fig. 9(b)–(d)) indicates the presence of α′ phase, due to its acicular morphology (Bartolomeu et al., 2017c; Zhang et al., 2014).

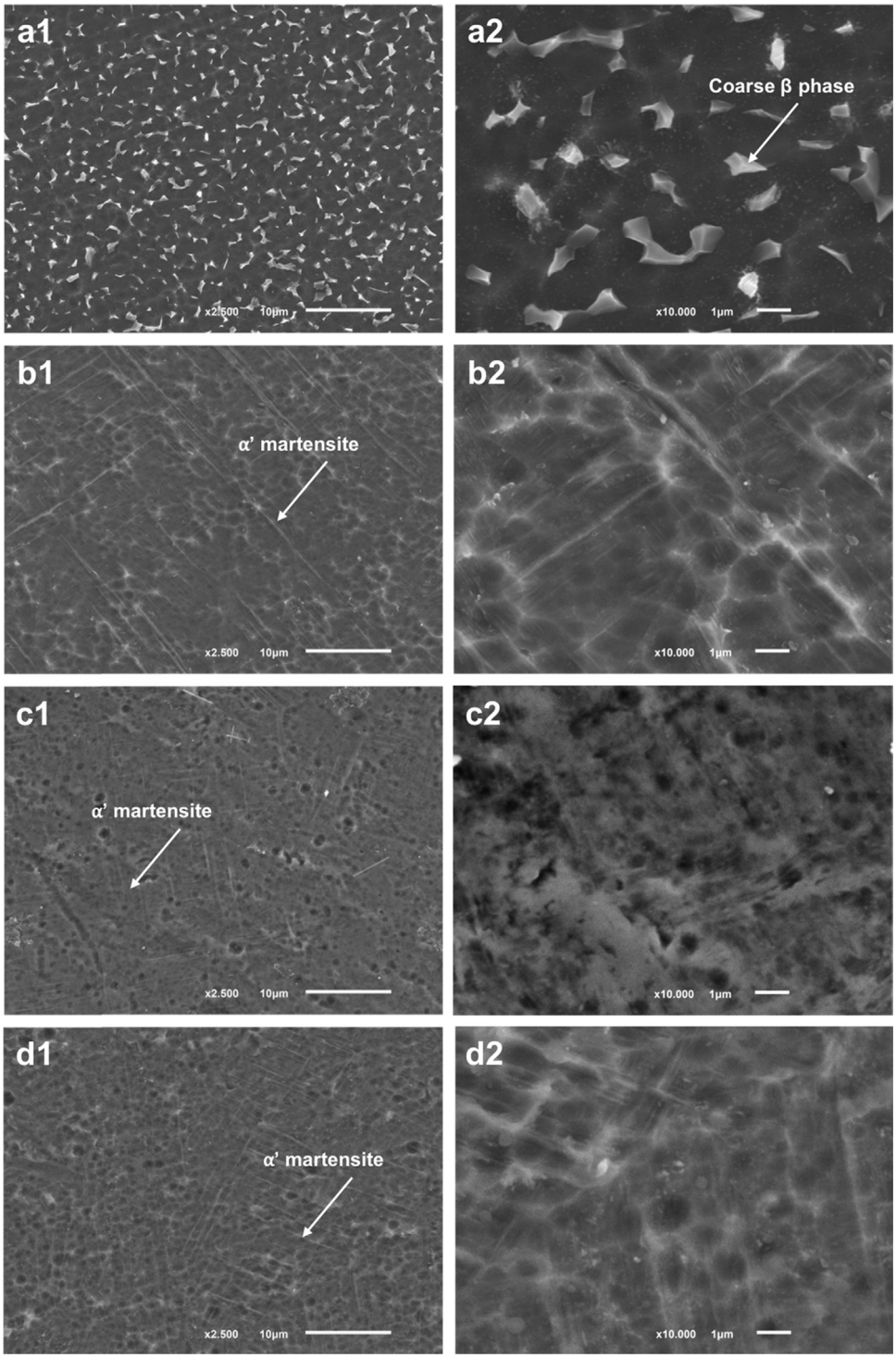

Fig. 9. SEM micrographs of the top surfaces of polished/acid-etched Ti6Al4V polished specimens: (a) SP1, (b) SP2, (c) SP3 and (d) Ti6Al4V-PEEK (acquired in a Ti6Al4V zone).

3.2. Evolution of the open circuit potential (OCP) and coefficient of friction (COF)

Fig. 12 displays the evolution of OCP as a function of time before, during and after tribocorrosion test conducted on SP1, SP2, SP3 and SP4 Ti6Al4V-based specimens.

Before sliding, when any load is applied, the OCP value of all the Ti6Al4V-based in all the tests was stabilized in order to assure the formation of a stable passive fill on the surfaces (Totolin et al., 2016). When the load is applied and the reciprocating sliding starts, the OCP immediately dropped down indicating the damage on the passive film and the exposure of the fresh surface to the electrolyte (called de-passivation) (Buciumeanu et al., 2017b). This behavior could be seen on all the specimens tested. On other hand, immediately after reaching the end of the reciprocating sliding (around 2000s), when the movement ends and the load is removed, the OCP values return back to values similar to those detected during the stabilization time. This behavior indicates the capability of all the specimens to regain their passive film, phenomenon called repassivation (Runa et al., 2013).

Considering the OCP average value during the sliding stage

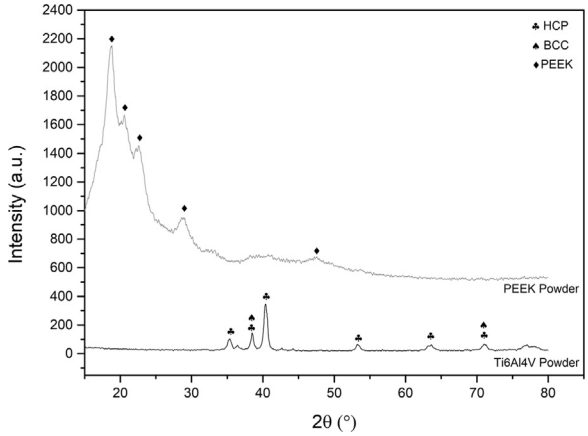

Fig. 10. Ti6Al4V and PEEK starting materials X-ray diffraction spectra.

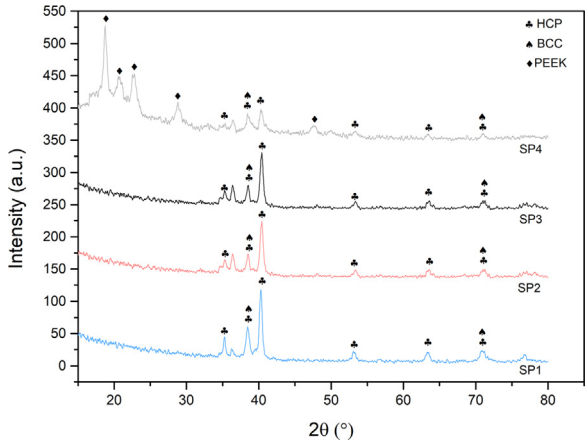

Fig. 11. SP1, SP2, SP3 and SP4 Ti6Al4V-based specimens X-ray diffraction spectra.

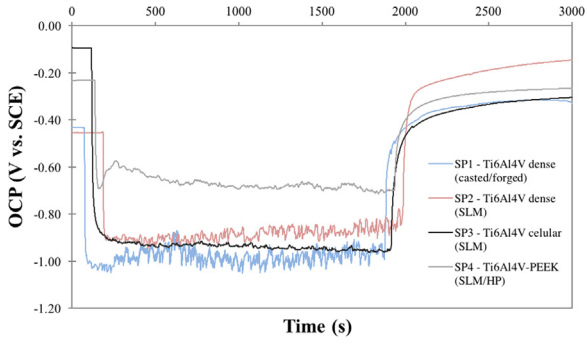

Fig. 12. Evolution of OCP recorded before, during and after sliding for SP1, SP2, SP3 and SP4 specimens.

(Fig. 12), some relevant differences between the different specimens can be detected. A cyclic passivation and repassivation process can be seen for all the specimens. The OCP values for SP1, SP2 and SP3 drop down until values around 0.91 ± 0.05 V. Similar values were reported elsewhere for Ti6Al4V specimens under dry tribocorrosion tests in reported studies (Buciumeanu et al., 2017a; Doni et al., 2013). In the case of SP4, the multi-material Ti6Al4V-PEEK structure, this decrease was significantly lower (values around 0.63 ± 0.02 V). The lower OCP value obtained for the multi-material (SP4), indicates that the presence of PEEK into the cellular structures, improved the corrosion behavior when compared to SP1, SP2 and SP3 under the tested conditions.

The synergistic interactions between wear and corrosion in this study are a combination of several aspects: exposed area to electrolyte, the area subjected to sliding, materials microstructure and hardness (induced by the processing routes). These aspects interaction is not well described in the available literature, being difficult to state which is the prevailing mechanism during the tribocorrosion process. In SP1 and SP2 the Ti6Al4V exposed area to electrolyte is around 63 mm^2, while for SP3 this value is around 135 mm^2 (considering all the areas on the open-cells). For SP4, the Ti6Al4V exposed area is around 47 mm^2 and the PEEK exposed area is around 16 mm^2. These differences can explain the dissimilarities observed on the passivation/repassivation process during sliding. The smaller area of exposed Ti6Al4V corresponded to the lowest tendency to corrosion, as shown by the lower OCP value during sliding. Ti6Al4V specimens produced by SLM (SP2, SP3 and SP4) are expected to show an unfavorable corrosion resistance comparing to SP1, once the dominant phases obtained using this process are α and α′ phases contrarily to SP1 (forged specimen) in which β-phase is the dominant (de Damborenea et al., 2017; Dai et al., 2016). On the other hand, SLM technique promotes an increase on the hardness of Ti6Al4V compared to forged specimens (Bartolomeu et al., 2016; Song et al., 2015) and consequently an increase on wear resistance (Bartolomeu et al., 2017c) that can enhance tribocorrosion performance. Another aspect to highlight is the exposed area during sliding. In the case of SP3, due to the presence open-cells, in each passage of the alumina ball, this area is approximately 25% lower when compared to SP1 and SP2. In the case of SP4, this 25% void area is filled with PEEK, that presents a very distinctive behavior from Ti6Al4V, highlighting its lubricating effect (Chen et al., 2012).

When regarding COF, Fig. 13 shows COF evolution during sliding and Table 3 the average values obtained regarding Ti6Al4V-bases specimens sliding against alumina. Firstly, no significant differences can be detected in regarding to SP1, SP2 and SP3. In fact, when measuring the COF of Ti6Al4V-alumina ball tribological pair, values close to 0.4 have been reported in other studies (Bartolomeu et al., 2017a,c; Chen et al., 2014). When regarding the multi-material Ti6Al4V-PEEK specimen (SP4) it can be noticed that the average value (0.362) is slightly lower that the obtained for the others specimens. This tendency can be related with the presence of the PEEK in active surface of the reciprocating sliding. M. Sampaio et al. (Sampaio et al., 2016a, b) performed tribological/tribocorrosion tests on PEEK specimens against alumina balls in lubricated conditions (artificial saliva) and obtained COF values around 0.1. In the present study, the COF value displayed by SP4 is slightly lower than the other specimen groups once PEEK is present on only approximately 25% of the surface area and although having a contribution towards the lowering of COF, Ti6Al4V is the predominant material in this tribological interaction.

Fig. 14 shows representative SEM images of the alumina ball that were slide against SP1, SP2, SP3 and SP4 specimens during the sliding stage on the tribocorrosion tests. By analyzing Table 3, it is noticed that the effect of the presence of PEEK on COF is low, i.e., it is lower than the expected considering the COF values of PEEK specimens in other studies (Sampaio et al., 2016a). This aspect can be understood by analyzing Fig. 14, in which the Ti6Al4V tribolayer that adheres to the alumina ball surface is present in all the specimens. This tribolayer can be responsible for disguised the effect of PEEK on COF, justifying the slight decrease on COF found for SP4 tests. By using Energy Dispersive Spectrometer technique was possible to confirm the presence of Titanium, Aluminum and Vanadium elements coming from the Ti6Al4V-based specimens on all the alumina balls.

3.3. Specific wear rate and surface morphologies after tribocorrosion tests

In Fig. 15 depicts the specific wear rate average values obtained for all the Ti6Al4V-based specimens tested against alumina balls.

By analyzing the experimental results obtained for the specific wear rate, can be concluded that significant differences were detected between all the different specimens. Ti6Al4V cellular structures (SP3),

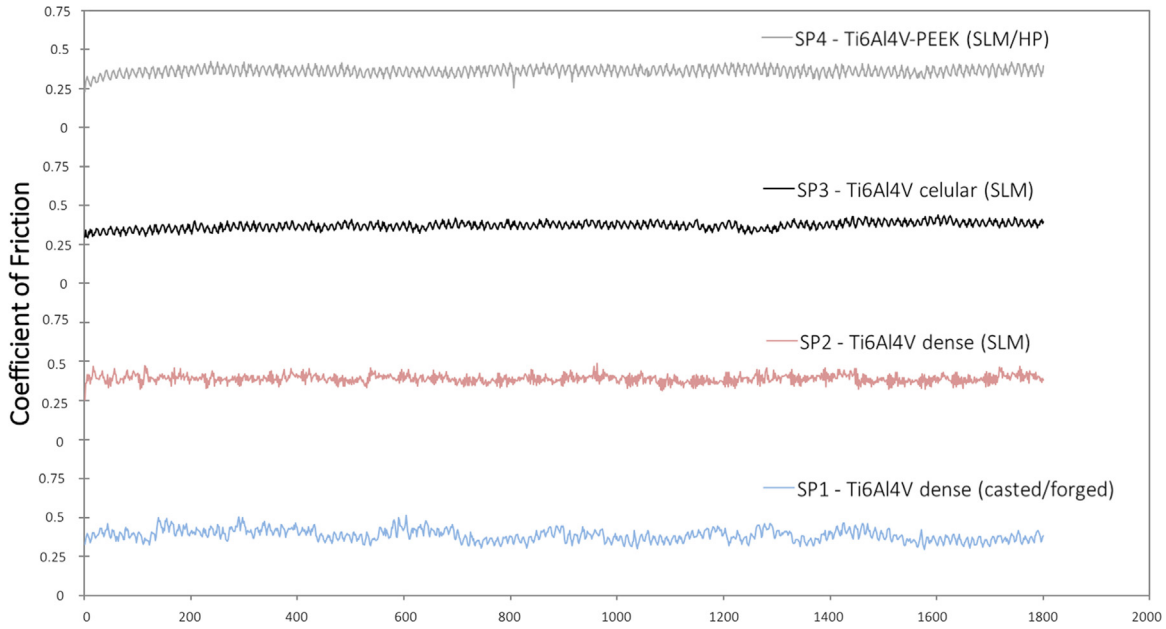

Fig. 13. Evolution of coefficient of friction for SP1, SP2, SP3 and SP4 specimens.

Table 3
Coefficient of friction mean values of Ti6Al4V-based specimens during reciprocating sliding.

Specimen	Coefficient of friction
SP1	0.395 ± 0.01
SP2	0.389 ± 0.01
SP3	0.417 ± 0.04
SP4	0.362 ± 0.02

exhibits the worst wear resistance (higher value of specific wear rate, k = $1.3E^{-03}$ mm^3N^{-1} m^{-1}). This result can be explained based on the presence of the open-cells (regions without material) that increase the contact pressure (Bartolomeu et al., 2017c; Fellah et al., 2014). In other words, for the same applied load there is a smaller area under loading (minus 25%), thus leading to higher contact pressure on SP3 specimens, when compared to SP1 and SP2 (dense specimens) and also to SP4 (where PEEK is present in the open-cells). When comparing SP2 (SLM) with SP1 (forged - the current material used in orthopedic applications (e.g. hip implants and tibial plates)) a 64% decrease on the specific

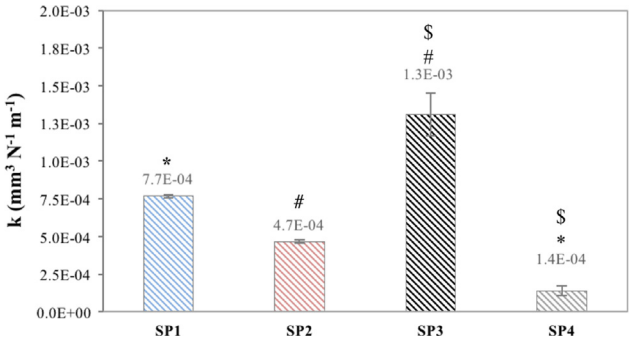

Fig. 15. Specific wear rate of Ti6Al4V- based specimens SP1, SP2, SP3 and SP4 against alumina normal load of 6 N at a frequency of 1 Hz and 3 mm of stroke length in Phosphate Buffer Solution at 37 °C. Symbols denote statistically significant differences ($p < 0.05$) as follows: (*) SP1 and SP4; (#) SP2 and SP3; ($) SP3 and SP4.

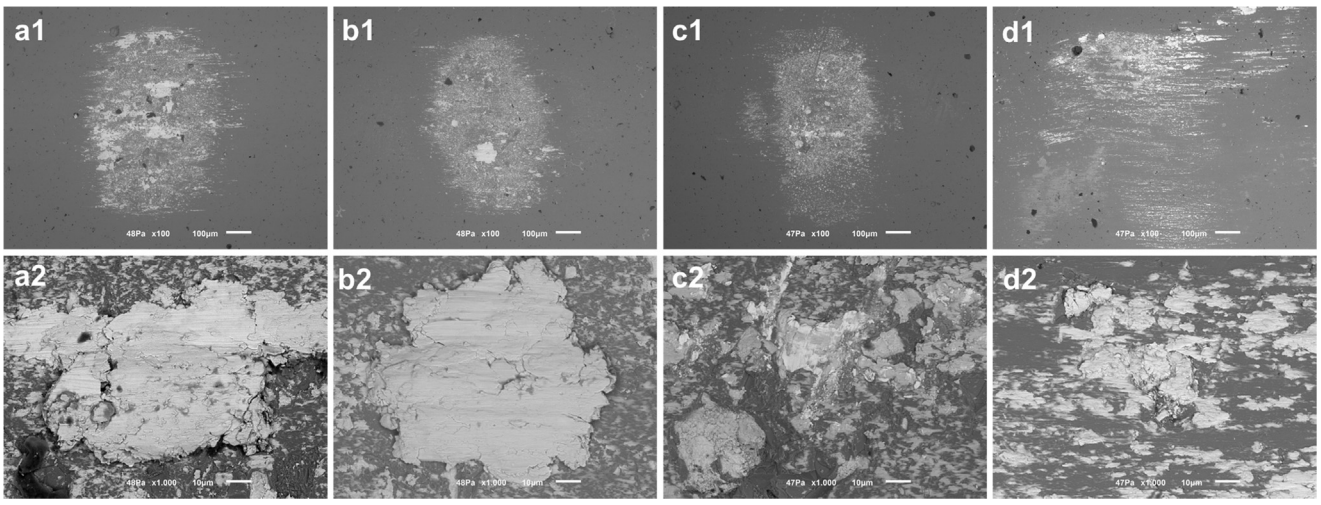

Fig. 14. SEM images of the alumina balls surface that was exposed to sliding against: (a) SP1; (b) SP2; (c) SP3; (d) SP4.

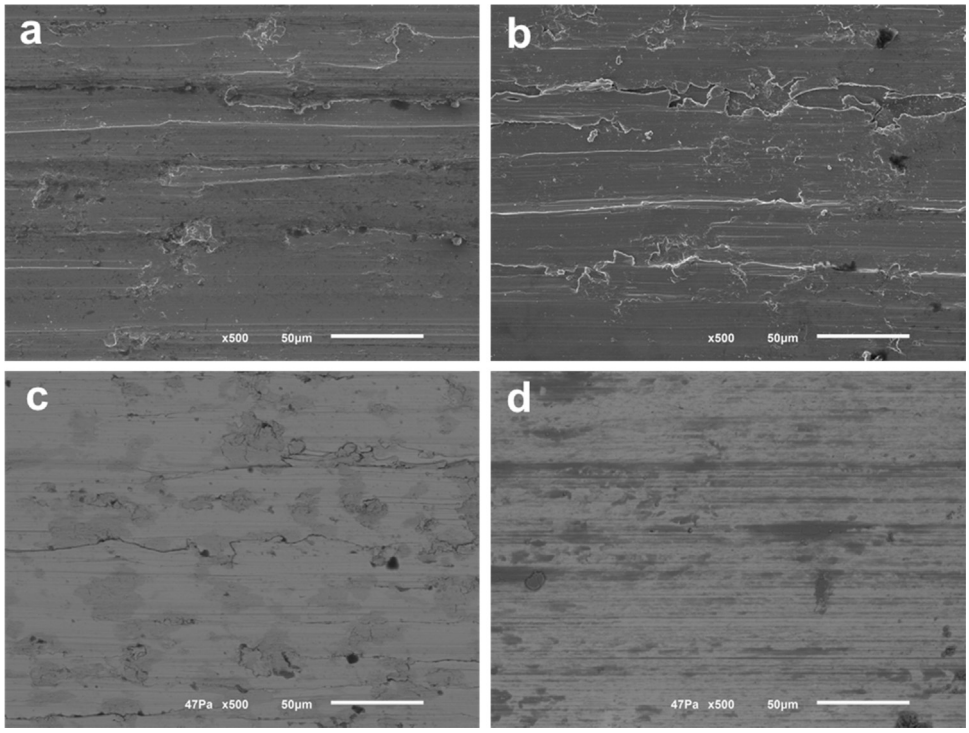

Fig. 16. SEM micrographs of top surfaces TiAl4V specimens after tribocorrosion tests: (a) SP1 (b) SP2; (c) SP3 (d) SP4.

wear rate was verified. This finding can be explained based on the differences on the microstructural features of these two materials, once the fine microstructure present on SP2 and also the presence of α′ martensite phase have been reported to increase the strength and hardness of Ti6Al4V produced by SLM when compared to forged (Bartolomeu et al., 2016; Song et al., 2015). Multi-material Ti6Al4V-PEEK (SP4) displays an expressive 450% decrease on the specific wear rate when compared to SP1 – that the represents the current solution used on orthopedic applications. When comparing this multi-material solution with the cellular structure obtained by SLM (SP3), an outstanding 829% decrease on the specific wear rate was found. In this sense, as observed for OCP values obtained during sliding (Fig. 12) and slightly for COF values (Fig. 13 and Table 3), the presence of PEEK significantly increases the wear resistance of these materials when compared to the other tested solutions.

Fig. 16 shows SEM images of all the systems after the tribocorrosion tests, where the wear mechanisms that were present during the sliding against alumina ball are visible. By analyzing these wear tracks, plastic deformation and abrasive grooves parallel to the reciprocating sliding direction can be observed for all the specimens tested. These abrasion grooves are created by the alumina, being a consequence of abrasive wear mechanisms occurring during sliding. Several works have been performed in which PEEK is used as coating to improve wear resistance (Sampaio et al., 2016b; Souza et al., 2015b; Wang and Terrell, 2013). In this study, a similar effect was obtained when introducing PEEK in the open-cells of Ti6Al4V cellular structures, once a significant higher wear resistance was obtained for Multi-material Ti6Al4V-PEEK when compared to all the other solutions tested. This outcome proves that the developed multi-material Ti6Al4V-PEEK cellular structure is a promising solution to be used in dental or orthopedic applications, owing to a superior performance when compared to the current solution used in commercially available implants/prosthesis/devices.

When regarding wear performance, these author's reported (Buciumeanu et al., 2018) superior wear resistance of Ti6Al4V-PEEK cellular structures when compared to Ti6Al4V cellular structures for different open-cells sizes and also when compared with Ti6Al4V dense materials. This study allowed to understand the highly positive effect of PEEK on porous structures considering wear resistance. In the present study, by combining SLM and HP was possible to produce Ti6Al4V-PEEK multi-material cellular structures that besides an improved wear resistance (with a reduction on the specific wear rate of 450% comparing to the material conventionally used in implants), also demonstrate a lower tendency to corrosion when compared to mono-material specimens, either dense or cellular structures. In the author's opinion the trade-off between the costs and the benefits of using HP after producing Ti6Al4V cellular structures by SLM is positive, especially for the fabrication of customized implant, that have already a high cost, due to the scanning of the patient anatomy.

4. Conclusions

The following detailed conclusions can be drawn from this work: . Ti6Al4V interconnected cellular structures were successfully produced by Selective Laser Melting technique;. The procedure to impregnate PEEK into the open-cells of the Ti6Al4V cellular structures by means of Hot Pressing was well-succeeded allowing to produce a multi-material Ti6Al4V-PEEK cellular structure;. The tribocorrosion behavior of multi-material Ti6Al4V-PEEK structure was assessed and significant differences were obtained when compared to the other groups studied;. The introduction of PEEK into TiAl4V cellular structures open-cells decreases the OCP value during sliding and increases the wear resistance;. The multi-material Ti6Al4V-PEEK cellular structure designed in this work, besides being able to withstand the loads occurring after implantation also enhances expressively the tribocorrosion performance, thus being a promising alternative to fully dense metals currently used on these applications.

Acknowledgements

This work was supported by FCT through the grants SFRH/BD/128657/2017 and SFRH/BPD/112111/2015, the project PTDC/EMS-TEC/5422/2014 and also by project NORTE 01–0145_FEDER-000018. Additionally, this work was supported by FCT with the reference project UID/EEA/04436/2013, by FEDER funds through the COMPETE

2020 – Programa Operacional Competitividade e Internacionalização (POCI) with the reference project POCI-01–0145-FEDER-006941.

References

Bartolomeu, F., Faria, S., Carvalho, O., Pinto, E., Alves, N., Silva, F.S., Miranda, G., 2016. Predictive models for physical and mechanical properties of Ti6Al4V produced by selective laser melting. Mater. Sci. Eng. A 663, 181–192. https://doi.org/10.1016/j.msea.2016.03.113.

Bartolomeu, F., Sampaio, M., Carvalho, O., Pinto, E., Alves, N., Gomes, J.R., Silva, F.S., Miranda, G., 2017a. Tribological behavior of Ti6Al4V cellular structures produced by selective laser melting. J. Mech. Behav. Biomed. Mater. 69, 128–134. https://doi.org/10.1016/j.jmbbm.2017.01.004.

Bartolomeu, F., Buciumeanu, M., Pinto, E., Alves, N., Carvalho, O., Silva, F.S., Miranda, G., 2017b. 316L stainless steel mechanical and tribological behavior—A comparison between selective laser melting, hot pressing and conventional casting. Addit. Manuf. 16, 81–89. https://doi.org/10.1016/j.addma.2017.05.007.

Bartolomeu, F., Buciumeanu, M., Pinto, E., Alves, N., Silva, F.S., Carvalho, O., Miranda, G., 2017c. Wear behavior of Ti6Al4V biomedical alloys processed by selective laser melting, hot pressing and conventional casting (English Ed.). Trans. Nonferrous Met. Soc. China 27, 829–838. https://doi.org/10.1016/S1003-6326(17)60060-8.

Bruschi, S., Bertolini, R., Ghiotti, A., 2017. Tribology International Coupling machining and heat treatment to enhance the wear behaviour of an additive manufactured Ti6Al4V titanium alloy. Tribol. Int. 116, 58–68. https://doi.org/10.1016/j.triboint.2017.07.004.

Buciumeanu, M., Araujo, A., Carvalho, O., Miranda, G., Souza, J.C.M., Silva, F.S., Henriques, B., 2017a. Study of the tribocorrosion behaviour of Ti6Al4V – HA biocomposites. Tribol. Int. 107, 77–84. https://doi.org/10.1016/j.triboint.2016.11.029.

Buciumeanu, M., Araujo, A., Carvalho, O., Miranda, G., Souza, J.C.M., Silva, F.S., 2017b. Tribology International study of the tribocorrosion behaviour of Ti6Al4V – HA biocomposites. Tribiol. Int. 107, 77–84. https://doi.org/10.1016/j.triboint.2016.11.029.

Buciumeanu, M., Almeida, S., Bartolomeu, F., Costa, M.M., Alves, N., Silva, F.S., Miranda, G., 2018. Ti6Al4V cellular structures impregnated with biomedical PEEK - New material design for improved tribological behavior. Tribol. Int. 119, 157–164. https://doi.org/10.1016/j.triboint.2017.10.038.

Chen, B., Wang, J., Yan, F., 2012. Comparative investigation on the tribological behaviors of CF/PEEK composites under sea water lubrication. Tribol. Int. 52, 170–177. https://doi.org/10.1016/j.triboint.2012.03.017.

Chen, J., Zhang, Q., Li, Q.A., Fu, S.L., Wang, J.Z., 2014. Corrosion and tribocorrosion behaviors of AISI 316 stainless steel and Ti6Al4V alloys in artificial seawater (English Ed.). Trans. Nonferrous Met. Soc. China 24, 1022–1031. https://doi.org/10.1016/S1003-6326(14)63157-5.

Dai, N., Zhang, L.C., Zhang, J., Chen, Q., Wu, M., 2016. Corrosion behavior of selective laser melted Ti-6Al-4 V alloy in NaCl solution. Corros. Sci. 102, 484–489. https://doi.org/10.1016/j.corsci.2015.10.041.

de Damborenea, J.J., Arenas, M.A., Larosa, M.A., Jardini, A.L., de Carvalho Zavaglia, C.A., Conde, A., 2017. Corrosion of Ti6Al4V pins produced by direct metal laser sintering. Appl. Surf. Sci. 393, 340–347. https://doi.org/10.1016/j.apsusc.2016.10.031.

Dantas, T.A., Abreu, C.S., Costa, M.M., Miranda, G., Silva, F.S., Dourado, N., Gomes, J.R., 2017. Bioactive materials driven primary stability on titanium biocomposites. Mater. Sci. Eng. C 77, 1104–1110. https://doi.org/10.1016/j.msec. 2017.04.014.

Donachie, MatthewJ., 2000. Titanium: A Technical Guide, 2nd Edition.

Donell, S.T., Darrah, C., Nolan, J.F., Wimhurst, J., Toms, A., Barker, T.H.W., Case, C.P., Tucker, J.K., 2010. Early failure of the Ultima metal-on-metal total hip replacement in the presence of normal plain radiographs. J. Bone Jt. Surg. - Br. 92–B, 1501–1508. https://doi.org/10.1302/0301-620X.92B11.24504.

Doni, Z., Alves, A.C., Toptan, F., Gomes, J.R., Ramalho, A., Buciumeanu, M., Palaghian, L., Silva, F.S., 2013. Dry sliding and tribocorrosion behaviour of hot pressed CoCrMo biomedical alloy as compared with the cast CoCrMo and Ti6Al4V alloys. Mater. Des. 52, 47–57. https://doi.org/10.1016/j.matdes.2013.05.032.

Fazel, M., Salimijazi, H.R., Golozar, M.A., Jazi, M.R. Garsivaz, 2015. A comparison of corrosion, tribocorrosion and electrochemical impedance properties of pure Ti and Ti6Al4V alloy treated by micro-arc oxidation process. Appl. Surf. Sci. 324, 751–756. https://doi.org/10.1016/j.apsusc.2014.11.030.

Fellah, M., Laba, M., Assala, O., Dekhil, L., Taleb, A., Rezag, H., Iost, A., 2014. Tribological behavior of Ti-6Al-4V and Ti-6Al-7Nb alloys for total hip prosthesis. Adv. Tribol. 2014.

Friedrich, K., Sue, H.J., Liu, P., Almajid, A.A., 2011. Scratch resistance of high performance polymers. Tribol. Int. 44, 1032–1046. https://doi.org/10.1016/j.triboint.2011.04.008.

Ganesh, B.K.C., Ramanaih, N., Rao, P.V. Chandrasekhar, 2012. Dry sliding wear behavior of Ti–6Al–4V implant alloy subjected to various surface treatments. Trans. Indian Inst. Met. 65, 425–434. https://doi.org/10.1007/s12666-012-0147-4.

Geetha, M., Singh, A.K., Asokamani, R., Gogia, A.K., 2009. Ti based biomaterials, the ultimate choice for orthopaedic implants - A review. Prog. Mater. Sci. 54, 397–425. https://doi.org/10.1016/j.pmatsci.2008.06.004.

Goodman, S.B., 2007. Wear particles, periprosthetic osteolysis and the immune system. Biomaterials 28, 5044–5048. https://doi.org/10.1016/j.biomaterials.2007.06.035.

Holzwarth, U., Cotogno, G., 2012. Total hip arthroplasty - state of the art, challenges and prospects. J. Bone Jt. Surg. Inc. https://doi.org/10.2788/31286.

Jovanović, M.T., Tadić, S., Zec, S., Mišković, Z., Bobić, I., 2006. The effect of annealing temperatures and cooling rates on microstructure and mechanical properties of investment cast Ti-6Al-4V alloy. Mater. Des. 27, 192–199. https://doi.org/10.1016/j.matdes.2004.10.017.

Kasperovich, G., Haubrich, J., Gussone, J., Requena, G., 2016. Correlation between porosity and processing parameters in TiAl6V4 produced by selective laser melting. Mater. Des. 105, 160–170. https://doi.org/10.1016/j.matdes.2016.05.070.

Licausi, M.P., Igual Muñoz, A., Amigó Borrás, V., 2013. Influence of the fabrication process and fluoride content on the tribocorrosion behaviour of Ti6Al4V biomedical alloy in artificial saliva. J. Mech. Behav. Biomed. Mater. 20, 137–148. https://doi.org/10.1016/j.jmbbm.2013.01.019.

Liu, Q., Wang, Y., Zheng, H., Tang, K., Ding, L., Li, H., Gong, S., 2016. Microstructure and mechanical properties of LMD-SLM hybrid forming Ti6Al4V alloy. Mater. Sci. Eng. A. 660, 24–33. https://doi.org/10.1016/j.msea.2016.02.069.

Liu, Y.J., Li, S.J., Wang, H.L., Hou, W.T., Hao, Y.L., Yang, R., Sercombe, T.B., Zhang, L.C., 2016. Microstructure, defects and mechanical behavior of beta-type titanium porous structures manufactured by electron beam melting and selective laser melting. Acta Mater. 113, 56–67. https://doi.org/10.1016/j.actamat.2016.04.029.

Lu, S.L., Qian, M., Tang, H.P., Yan, M., Wang, J., StJohn, D.H., 2016. Massive transformation in Ti-6Al-4V additively manufactured by selective electron beam melting. Acta Mater. 104, 303–311. https://doi.org/10.1016/j.actamat.2015.11.011.

Miranda, G., Faria, S., Bartolomeu, F., Pinto, E., Madeira, S., Mateus, A., Carreira, P., 2016. Predictive models for physical and mechanical properties of 316L stainless steel produced by selective laser melting. Mater. Sci. Eng. A 657, 43–56. https://doi.org/10.1016/j.msea.2016.01.028.

Moon, S.M., Ingalhalikar, A., Highsmith, J.M., Vaccaro, A.R., 2009. Biomechanical rigidity of an all-polyetheretherketone anterior thoracolumbar spinal reconstruction construct: an in vitro corpectomy model. Spine J. 9, 330–335. https://doi.org/10.1016/j.spinee.2008.11.012.

Murr, L.E., Quinones, S.A., Gaytan, S.M., Lopez, M.I., Rodela, A., Martinez, E.Y., Hernandez, D.H., Martinez, E., Medina, F., Wicker, R.B., 2009. Microstructure and mechanical behavior of Ti-6Al-4V produced by rapid-layer manufacturing, for biomedical applications. J. Mech. Behav. Biomed. Mater. 2, 20–32. https://doi.org/10.1016/j.jmbbm.2008.05.004.

Obadele, B.A., Andrews, A., Mathew, M.T., Olubambi, P.A., Pityana, S., 2015. Improving the tribocorrosion resistance of Ti6Al4V surface by laser surface cladding with TiNiZrO < inf > 2 < /inf > composite coating. Appl. Surf. Sci. 345, 99–108. https://doi.org/10.1016/j.apsusc.2015.03.152.

Raju, R., Duraiselvam, M., Petley, V., Verma, S., Rajendran, R., 2015. Microstructural and mechanical characterization of Ti6Al4V refurbished parts obtained by laser metal deposition. Mater. Sci. Eng. A 643, 64–71. https://doi.org/10.1016/j.msea.2015.07.029.

Rodrigues, D.C., Valderrama, P., Wilson, T.G., Palmer, K., Thomas, A., Sridhar, S., Adapalli, A., Burbano, M., Wadhwani, C., 2013. Titanium corrosion mechanisms in the oral environment: a retrieval study. Materials (Basel) 6, 5258–5274. https://doi.org/10.3390/ma6115258.

Runa, M.J., Mathew, M.T., Rocha, L.A., 2013. Tribocorrosion response of the Ti6Al4V alloys commonly used in femoral stems. Tribol. Int. 68, 85–93. https://doi.org/10.1016/j.triboint.2013.09.022.

Sampaio, M., Buciumeanu, M., Henriques, B., Silva, F.S., Souza, J.C.M., Gomes, J.R., 2016a. Tribocorrosion behavior of veneering biomedical PEEK to Ti6Al4V structures. J. Mech. Behav. Biomed. Mater. 54, 123–130. https://doi.org/10.1016/j.jmbbm.2015.09.010.

Sampaio, M., Buciumeanu, M., Askari, E., Flores, P., Souza, J.C.M., Gomes, J.R., Silva, F.S., Henriques, B., 2016b. Effects of poly-ether-ether ketone (PEEK) veneer thickness on the reciprocating friction and wear behavior of PEEK/Ti6Al4V structures in artificial saliva. Wear 368–369, 84–91. https://doi.org/10.1016/j.wear.2016.09.009.

Shunmugavel, M., Polishetty, A., Littlefair, G., 2015. Microstructure and mechanical properties of wrought and additive manufactured Ti-6Al-4V cylindrical bars. Procedia Technol. 20, 231–236. https://doi.org/10.1016/j.protcy.2015.07.037.

Song, B., Zhao, X., Li, S., Han, C., Wei, Q., Wen, S., Liu, J., Shi, Y., 2015. Differences in microstructure and properties between selective laser melting and traditional manufacturing for fabrication of metal parts: a review. Front. Mech. Eng. 10, 111–125. https://doi.org/10.1007/s11465-015-0341-2.

Souza, J.C.M., Henriques, M., Teughels, W., Ponthiaux, P., Celis, J.-P., Rocha, L.A., 2015a. Wear and corrosion interactions on titanium in oral environment: literature review. J. Bio- Tribo-Corros. 1, 13. https://doi.org/10.1007/s40735-015-0013-0.

Souza, J.C.M., Tajiri, H.A., Morsch, C.S., Buciumeanu, M., Mathew, M.T., Silva, F.S., Henriques, B., 2015b. Tribocorrosion behavior of Ti6Al4V coated with a bio-absorbable polymer for biomedical applications. J. Bio- Tribo-Corros. 1, 2–7. https://doi.org/10.1007/s40735-015-0029-5.

Thijs, L., Verhaeghe, F., Craeghs, T., Van Humbeeck, J., Kruth, J.P., 2010. A study of the microstructural evolution during selective laser melting of Ti-6Al-4V. Acta Mater. 58, 3303–3312. https://doi.org/10.1016/j.actamat.2010.02.004.

Toh, W., Wang, P., Tan, X., Nai, M., Liu, E., Tor, S., 2016. Microstructure and wear properties of electron beam melted Ti-6Al-4V parts: a comparison study against As-cast form. Metals (Basel) 6, 284. https://doi.org/10.3390/met6110284.

Totolin, V., Pejakovi, V., Csanyi, T., Hekele, O., Huber, M., Rodríguez, M., 2016. Surface engineering of Ti6Al4V surfaces for enhanced tribocorrosion performance in arti ficial seawater. Mater. Des. 104, 10–18. https://doi.org/10.1016/j.matdes.2016.04.080.

Van Hooreweder, B., Apers, Y., Lietaert, K., Kruth, J.P., 2017. Improving the fatigue performance of porous metallic biomaterials produced by Selective Laser Melting. Acta Biomater. 47, 193–202. https://doi.org/10.1016/j.actbio.2016.10.005.

Wang, X., Xu, S., Zhou, S., Xu, W., Leary, M., Choong, P., Qian, M., Brandt, M., Xie, Y.M., 2016. Topological design and additive manufacturing of porous metals for bone scaffolds and orthopaedic implants: a review. Biomaterials 83, 127–141. https://doi.org/10.1016/j.biomaterials.2016.01.012.

Wang, Y., Terrell, E.J., 2013. Influence of coating thickness and substrate elasticity on the

tribological performance of PEEK coatings. Wear 303, 255–261. https://doi.org/10.1016/j.wear.2013.03.036.

Weißmann, V., Wieding, J., Hansmann, H., Laufer, N., Wolf, A., Bader, R., 2016. Specific yielding of selective laser-melted Ti6Al4V open-porous scaffolds as a function of unit cell design and dimensions. Metals (Basel) 6, 166. https://doi.org/10.3390/met6070166.

Xu, W., Brandt, M., Sun, S., Elambasseril, J., Liu, Q., Latham, K., Xia, K., Qian, M., 2015. Additive manufacturing of strong and ductile Ti-6Al-4V by selective laser melting via in situ martensite decomposition. Acta Mater. 85, 74–84. https://doi.org/10.1016/j.actamat.2014.11.028.

Zhang, S., Wei, Q., Cheng, L., Li, S., Shi, Y., 2014. Effects of scan line spacing on pore characteristics and mechanical properties of porous Ti6Al4V implants fabricated by selective laser melting. Mater. Des. 63, 185–193. https://doi.org/10.1016/j.matdes.2014.05.021.